Elastic scattering of ^{40}Ar and ^{84}Kr on ^{209}Bi and ^{238}U at 7.2 and 8.5 MeV/N†

J. R. Birkelund* and J. R. Huizenga
Departments of Chemistry and Physics, University of Rochester, Rochester, New York 14627

H. Freiesleben
Fachbereich Physik, University of Marburg, Marburg, Germany
and Department of Chemistry and Physics, University of Rochester, Rochester, New York 14627

K. L. Wolf and J. P. Unik
Chemistry Division, Argonne National Laboratory, Argonne, Illinois 60439

V. E. Viola, Jr.
Cyclotron Laboratory and Chemistry Department, University of Maryland, College Park, Maryland 20742
(Received 10 September 1975)

Cross sections for elastic scattering of ^{40}Ar on targets of ^{209}Bi and ^{238}U were measured at energies of 286 and 340 MeV. Cross sections for the elastic scattering of ^{84}Kr on ^{209}Bi were measured at energies of 600 and 712 MeV. These experimental elastic scattering data were fitted with optical and Fresnel models. The total reaction cross section deduced from the Fresnel model by the one-quarter point technique agrees within a few percent with the result from the optical model. The Fresnel interaction radius and the optical model strong absorption radius are found to be approximately equal and qualitatively reproduced by the sum of the half-density electron scattering radii of the two heavy ions and a constant of 3.2 ± 0.3 fm. A method of estimating total reaction cross sections for heavy ions is presented. Some observations on the real and imaginary potentials of very heavy ions are presented.

[NUCLEAR REACTIONS ^{209}Bi(^{40}Ar, ^{40}Ar) and ^{238}U(^{40}Ar, ^{40}Ar) $E = 286$ MeV, $E = 340$ MeV, ^{209}Bi(^{84}Kr, ^{84}Kr) $E = 600$ MeV and $E = 712$ MeV. Measured elastic scattering cross section. Fitted optical and Fresnel models to the data. Deduced maximum angular momenta, interaction radii, and total reaction cross sections.]

I. INTRODUCTION

Recent investigations of the interaction of projectiles heavier than argon with heavy target nuclei have shown the importance of a new nuclear interaction mechanism.[1-6,10] In the determination of the cross sections for the various reaction mechanisms in heavy ion reactions, it is important to have an estimate of the total reaction cross section in order to determine the relative probability of each mode of interaction and to ensure that all possible partial reaction cross sections have been found. Estimates of the total reaction cross section can be made from the analysis of elastic scattering angular distributions using an optical model, or from strong absorption models which parametrize the partial wave reflection coefficients.[7] However, for very heavy ion reactions, where the Coulomb force is of similar magnitude to the nuclear force, an analytic expression for the elastic scattering angular distribution can be derived from a model based on a Fresnel scattering analysis.[8] In addition, the total reaction cross section can be calculated from the "quarter-point" technique.[9]

This paper describes measurements of the elastic scattering angular distributions for 286- and 340-MeV ^{40}Ar on ^{209}Bi and ^{238}U targets, and 600- and 712-MeV ^{84}Kr on ^{209}Bi. Analysis of the data using both the optical model and the Fresnel model is also described and the results of both types of analysis are compared. In addition, elastic scattering data for which optical model analyses are to be found in the literature [10-25] have been analyzed using the Fresnel model. The results of this analysis are compared with the published optical model analyses.

II. EXPERIMENTAL ARRANGEMENT

The elastic scattering of argon and krypton projectiles from bismuth and uranium were studied using superhilac accelerator. The targets were elemental Bi and anhydrous UF_4 line targets of approximately 3-mm × 7-mm size and 70–500 μg/cm^2 in thickness. The targets were prepared by vacuum evaporation onto 100-μg/cm^2 carbon backing foils, and mounted with the target material facing the detectors.

Particle detection was achieved with two silicon surface barrier detectors mounted on moveable

arms. One detector (referred to as the defining detector) was covered by a rectangular slit, subtending at the target 1° in the reaction plane and ±2.5° out of plane. The second detector was a position-sensitive detector which subtended a total of 25° in plane. The position-sensitive detector was covered with ten rectangular apertures each of which subtended 1° in plane and ±3.7° out of plane. The inherent position resolution of the position-sensitive detector corresponded to an angular resolution in the laboratory system of ~0.5°. The error in the angular position of each detector was less than ±0.5°. Each detector aperture was covered by a 0.132-mg/cm² Ni foil in order to suppress background. In addition, electron suppression was achieved for the position-sensitive detector by a vertical 4-kV potential between two horizontal metal plates placed in front of the detector aperture.

Elastic scattering events were detected in both detectors in a singles mode and recorded on magnetic tape for off-line data analysis. Beam monitor counters consisted of two silicon surface barrier detectors mounted at ±25° from the beam, and 15° above the reaction plane. Counts in the monitor detectors were used to determine left-right changes in beam direction and for cross section normalization.

Signals from a pulse generator were fed into the detector preamplifier during the beam pulses. The system live time was obtained by comparing the counts in the pulser peak in the recorded pulse spectrum with the number of pulses counted by an ungated scaler connected directly to the pulse generator. The pulsing system was not available for live time correction in the case of the ^{84}Kr results at 600 MeV. However, the relative Kr elastic scattering angular distribution could be obtained from the particle energy spectrum obtained at different positions in the position-sensitive detector. This was done over the range $41.6° < \theta_{c.m.} < 74.3°$, which was subtended by the position-sensitive detector at a single angular setting. For such a measurement, the live time, although unmeasured, is the same for particles detected at all angles within the range of the position-sensitive detector. In order to be certain that the dead time did not distort the measurements, the beam current was limited to keep the dead time below ~20% and measurements were made at several values of beam current. For all angular distributions other than Kr+Bi at 600 MeV, the data consist of measurements made using the defining detector at several angles, and the position-sensitive detector at a few angular settings. Normalization of the ratio $\sigma_{el}/\sigma_{Ruth}$ obtained from the position-sensitive detector to the ratio found using the defining detector is effected in two ways. (a) If the position-sensitive detector subtends an angular range such that counts in some of the most forward slits should lead to a ratio $\sigma_{el}/\sigma_{Ruth} = 1$, then the normalization of the position-sensitive detector measurements is obtained by setting the average value of the ratio $\sigma_{el}/\sigma_{Ruth}$ equal to one at the most forward angles for which measurements are made. (b) In cases where the position-sensitive detector is not sufficiently far forward to lead to $\sigma_{el}/\sigma_{Ruth} = 1$ at some of the slit positions, then the data from the position-sensitive detector are normalized using the cross section ratios obtained from the defining detector.

III. RESULTS

The experimental ratios of elastic to Rutherford scattering cross sections $\sigma_{el}/\sigma_{Ruth}(\theta_{c.m.})$ for ^{40}Ar at 286 and 340 MeV on ^{209}Bi and ^{238}U and ^{84}Kr at 600 and 712 MeV on ^{209}Bi are shown in Figs. 1–6. The errors include the statistical errors and an estimate of the errors introduced in separating elastically scattered particles from the inelastic and few nucleon transfer events in the energy spectrum. This problem of separation of elastic and inelastic events arises near the angle corresponding to a grazing collision. In this case separ-

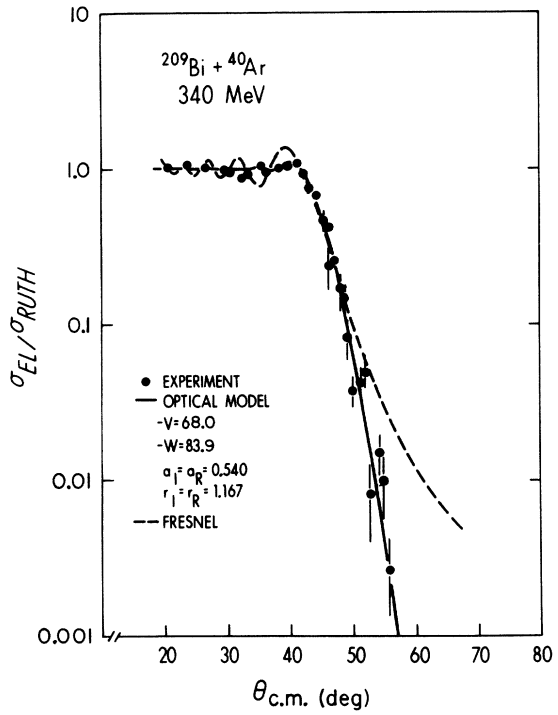

FIG. 1. Ratios of the experimental elastic scattering cross section to the Rutherford cross section as a function of the center-of-mass angle θ for the ^{209}Bi + ^{40}Ar reaction at 340 MeV (laboratory energy). The dashed and solid lines are Fresnel and optical model fits, respectively, to the data.

ation has been effected by obtaining a standard elastic peak shape from the spectrum at an angle sufficiently forward to be unaffected by inelastic and transfer events, but not so far forward as to be affected by resolution degradation brought about by high count rates. The standard peak shape is then fitted to the elastic peak at angles near the grazing angle in order to extract the integrated count of elastic events. The use of this fitting procedure is illustrated in Fig. 7 for the reaction of 712-MeV ^{84}Kr on ^{209}Bi. In this case the standard peak is the 18.5° run. The experimental data (points) at angles 38.8, 46.4, and 54° are compared with the standard peak (solid curve obtained from 18.5° spectrum) in the three right panels of Fig. 7. The experimental spectra and solid curves at the above three angles illustrate the peak fitting and unfolding procedure for a forward angle, an angle near the grazing angle, and a very backward angle. The full width at half maximum (FWHM) of the standard peak corresponded to an energy resolution of $\leq 2\%$ for the defining detectors and 2–6% for the position-sensitive detectors.

For the ^{40}Ar data discussed in this paper, at angles near the quarter-point angle ($\theta_{1/4}$) where $\sigma_{el}/\sigma_{Ruth} = 0.25$, the number of transfer events in the peaks is approximately equal to the number of elastic events. At angles separated from $\theta_{1/4}$ by more than 10° the transfer events are negligible. For the ^{84}Kr data the separation of elastic events from the spectrum is even more difficult since the beam energy is higher than that for the ^{40}Ar data and hence the 2% detector energy resolution corresponds to a larger energy range. The problem of inadequate resolution is even more acute in the position-sensitive detector. An estimate of the errors introduced because of the transfer events is not obtained for ^{84}Kr measurements as easily as for ^{40}Ar measurements since (near $\theta_{1/4}$) the tail on the elastic peak in the spectrum extends into the peak produced by strongly damped collisions which have a large cross section for ^{84}Kr incident on ^{209}Bi. Hence, it is necessary to separate three different types of collision events in the spectrum. The errors in the elastic scattering cross section measurements for the ^{84}Kr projectile are probably about twice as large as the errors for the ^{40}Ar measurements but error estimation is more difficult in the ^{84}Kr case.

The elastic scattering data have been compared with the predictions of two different models: (a) The Fresnel scattering model and (b) the optical model.

A. Fresnel scattering model

The theory of this model has been discussed by Frahn[8] who shows that the ratio $\sigma_{el}/\sigma_{Ruth}(\theta_{c.m.})$ is given by

$$\frac{\sigma_{el}}{\sigma_{Ruth}}(\theta) = \tfrac{1}{2}\{[\tfrac{1}{2} - S(y)]^2 + [\tfrac{1}{2} - C(y)]^2\}, \quad (1)$$

where $S(y)$ and $C(y)$ are the Fresnel sine and cosine integrals. The argument y is

$$y = \left(\frac{2\eta}{\pi}\right)^{1/2} \csc\tfrac{1}{2}(\theta_{1/4}) \sin[\tfrac{1}{2}(\theta - \theta_{1/4})]. \quad (2)$$

The Coulomb parameter η is given by

$$\eta = \frac{Z_1 Z_2 e^2}{\hbar v}, \quad (3)$$

where $Z_1 e$ and $Z_2 e$ are the charges on the target and projectile and v is their relative velocity at large separations. The angle $\theta_{1/4}$ is the quarter-point angle obtained from the experimental angular distribution as the angle for which $\sigma_{el}/\sigma_{Ruth} = 0.25$.

In this model the maximum angular momentum l_{max} for a particle taking part in a reaction with the target is given by

$$l_{max} = \eta \cot(\tfrac{1}{2}\theta_{1/4}). \quad (4)$$

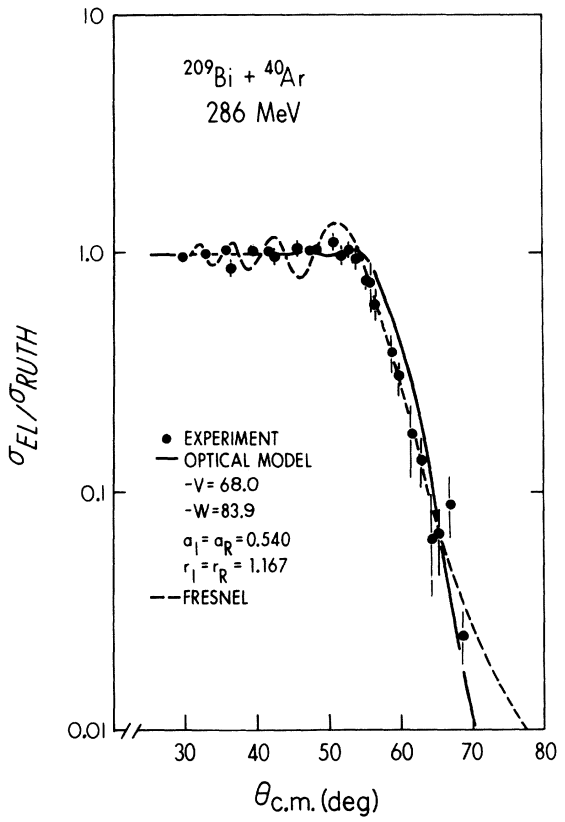

FIG. 2. Same as Fig. 1 except for the laboratory energy of 286 MeV.

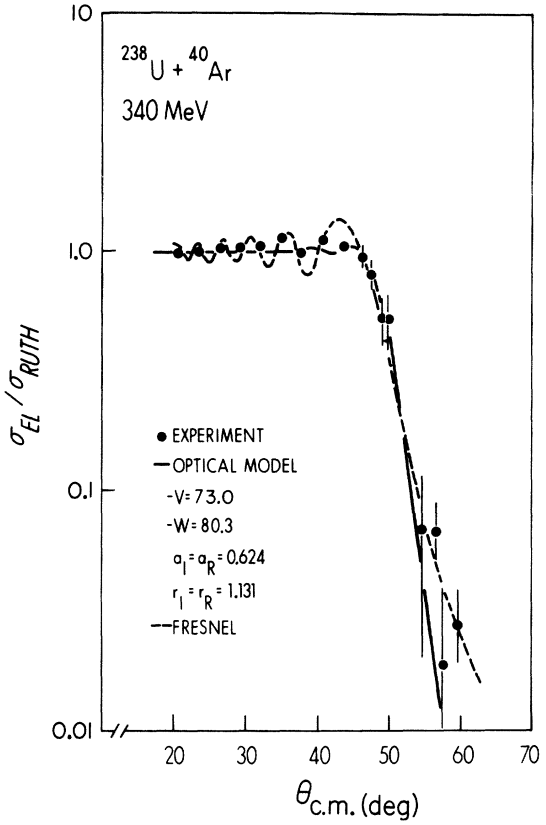

FIG. 3. Same as Fig. 1 except for the $^{238}U + ^{40}Ar$ reaction at 340 MeV (lab).

The interaction radius corresponds to

$$R_{int} = r_0 (A_p^{1/3} + A_T^{1/3}) = \frac{\eta}{k} [\csc(\tfrac{1}{2}\theta_{1/4}) + 1] . \quad (5)$$

The reaction cross section is given by

$$\sigma_R = \pi\lambda^2 (l_{max} + 1)^2 . \quad (6)$$

This model is supposed valid for the cases where

$$l_{max} >> 1 \text{ and } l_{max} \sin\theta_{1/4} \gtrsim 1. \quad (7)$$

Comparisons between the predictions of this model and the experimental data are shown in Figs. 1–6. The Fresnel parameters deduced from the data are given in Table I.

B. Optical model

The optical model search routine GENOA,[26] capable of handling 450 partial waves, has been used to find nuclear potentials which lead to a fit to the data for the elastic scattering angular distributions. The nuclear potential has a Woods-Saxon form and the total potential is given by

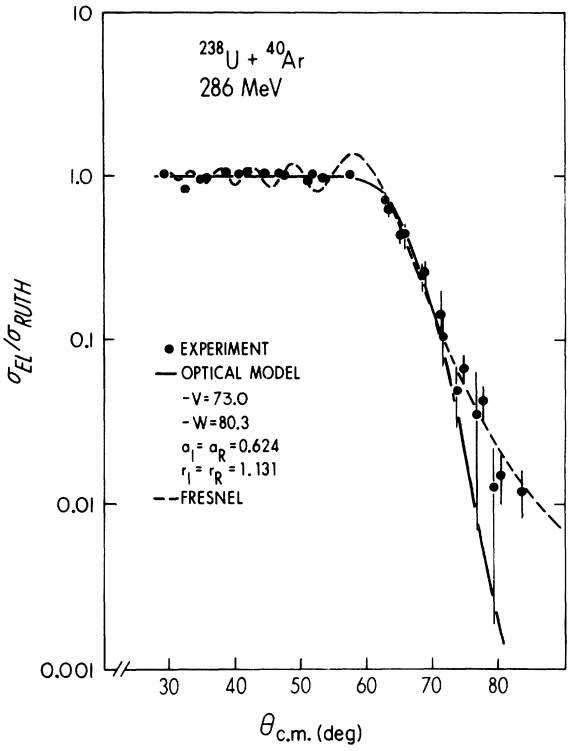

FIG. 4. Same as Fig. 1 except for the $^{238}U + ^{40}Ar$ reaction at 286 MeV (lab).

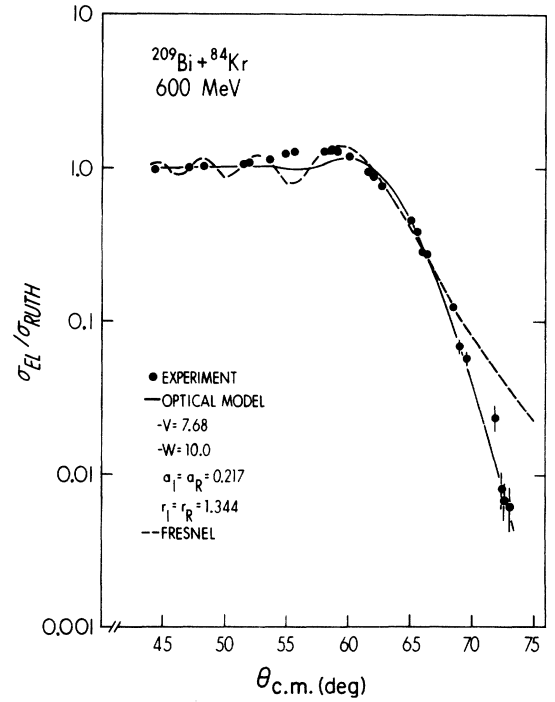

FIG. 5. Same as Fig. 1 except for the $^{209}Bi + ^{84}Kr$ reaction at 600 MeV (lab).

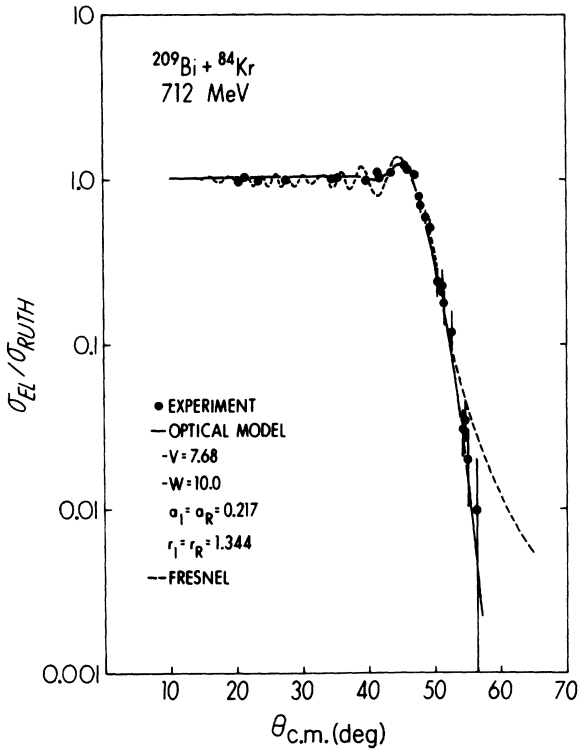

FIG. 6. Same as Fig. 1 except for the ^{209}Bi + ^{84}Kr reaction at 712 MeV (lab).

$$V(l,r) = V_C(r) + V_l(r) + (V + iW)\left[1 + \exp\left(\frac{r-R}{a}\right)\right]^{-1}, \tag{8}$$

where

$$R = r_{opt}[A_p^{1/3} + A_T^{1/3}]. \tag{9}$$

The Coulomb potential $V_C(r)$ is that of a spherical charge distribution

$$V_C(r) = \frac{Z_1 Z_2 e^2}{2R_C^3}(3R_C^2 - r^2), \quad r \le R_C$$

$$= \frac{Z_1 Z_2 e^2}{r}, \quad r > R_C, \tag{10}$$

$$R_C = r_C A_T^{1/3}. \tag{11}$$

The Coulomb radius parameter r_C was fixed at 1.4 fm for all calculations. The quantity $V_l(r)$ is the centrifugal potential.

For a given target the elastic scattering data at both energies were fitted with the same energy-independent parameters. Optical model potential parameters leading to the angular distributions shown in Figs. 1–6 are listed in Table II.

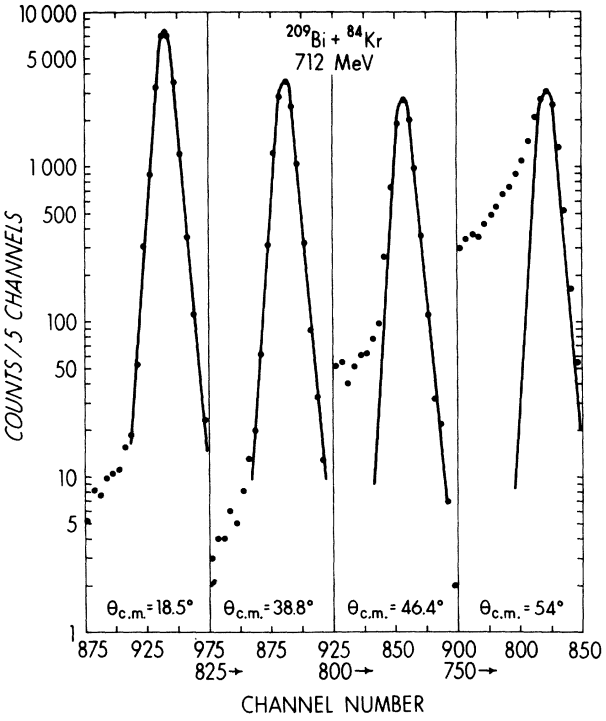

FIG. 7. Experimental elastic scattering spectra (points) at four angles for the reaction of 712-MeV ^{84}Kr on ^{209}Bi. The run at 18.5° is used as the standard spectrum. This spectrum is shown as a solid curve on the other three spectra. The angles 38.8°, 46.4°, and 54° represent a forward angle, an angle near the grazing angle, and a very backward angle, respectively. The counts in the 18.5° spectrum have been divided by 10.

IV. DISCUSSION

A. Comparison of results from Fresnel and optical models

Because η is large for the projectiles and energies used to obtain the data shown in Figs. 1–6, the elastic scattering angular distributions show a

TABLE I. Parameters deduced from the Fresnel scattering model fitted to the data of Figs. 1–6.

Target	E_{lab} (MeV)	η	$\theta^{c.m.}_{1/4}$ (deg)	r_0 [a] (fm)	l_{max}	σ_R (mb)
			^{40}Ar projectile			
^{209}Bi	340	80.63	47	1.411	185	2382
^{209}Bi	286	87.91	60	1.433	151	1887
^{238}U	340	89.37	51	1.414	187	2336
^{238}U	286	97.44	68	1.411	144	1648
			^{84}Kr projectile			
^{209}Bi	712	161.6	50.5	1.37	343	2533
^{209}Bi	600	175.9	66	1.38	270	1880

[a] r_0 is defined in terms of the quarter-point angle $\theta_{1/4}$ by Eq. (5).

classical Fresnel scattering shape. The ratios $\sigma_{el}/\sigma_{Ruth}$ are close to 1 (at forward angles) and fall exponentially without oscillation as θ increases. In all cases shown, the Fresnel model predictions for $\sigma_{el}/\sigma_{Ruth}(\theta)$ show larger oscillations at forward angles than are present in the data. However, the decrease in the ratios $\sigma_{el}/\sigma_{Ruth}$ near the quarter point are well reproduced over more than one order of magnitude. At angles for which $\sigma_{el}/\sigma_{Ruth} \lesssim 0.1$, the Fresnel model predicts elastic scattering cross sections which are usually too large.

The optical model curves fitted to the data reproduce the details of the experimental angular distributions somewhat better than the Fresnel model, especially at large scattering angles. However, by comparing the parameter values in Tables I and II, it can be seen that the maximum angular momentum l_{max} extracted from the Fresnel model using Eq. (4), is very close to the angular momentum $l_{1/2}$ for which the optical model transmission coefficient is 0.5. In addition, the reaction cross sections predicted by both the optical model and the Fresnel model agree for most cases to well within 10%. These properties are present for all the optical model parameter sets which have been tested.

If, in the data analysis, no correction is made for few nucleon transfer events in the spectrum, then the observed quarter-point angle will be too large and the corresponding reaction cross section will be too low. Since the analysis described in this paper estimates the contribution of transfer events in the energy spectrum, errors in the quarter-point angle are $\pm 1^\circ$ for the ^{40}Ar measurements and $^{+1}_{-2}{}^\circ$ for the ^{84}Kr measurements. These errors arise from the uncertainty in the detector positions and the problem of separating elastic and transfer events. The projectile energy uncertainty and errors in the quarter-point angle together lead to errors in the total reaction cross section of $\pm 5\%$ for the ^{40}Ar reactions and $^{+10}_{-5}\%$ for the ^{84}Kr reactions. However, because of the large corrections necessary for transfer and strongly damped events, the detailed shape of the elastic scattering angular distribution is not well determined by experiments with low or moderate energy resolution. In particular, for the case of ^{84}Kr + ^{209}Bi, if the transfer events are not separated completely from the elastic scattering events, then the calculated ratio $\sigma_{el}/\sigma_{Ruth}$ will show a rise at angles just forward of the falloff in the ratio. Such a rise in the ratio of $\sigma_{el}/\sigma_{Ruth}$ up to 1.9 before the falloff has been calculated by Rowley and attributed to the effects of the nuclear potential on the ion trajectories.[27] Experimental evidence quoted in support of such a large peak is the reported peak values[11] of $\sigma_{el}/\sigma_{Ruth}$ of 1.6 for the reaction of 500-MeV ^{84}Kr on targets of ^{208}Pb and ^{232}Th. However, careful analyses of experimental data of high resolution are necessary before the details of such an effect of the nuclear

TABLE II. Parameters for the optical model fit to the data displayed in Figs. 1–6.

Target	E_{lab} (MeV)	V (MeV)	r_R [a] (fm)	a_R [a] (fm)	W (MeV)	r_I [a] (fm)	a_I [a] (fm)	$l_{1/2}$	σ_R (mb)
				^{40}Ar projectiles					
^{209}Bi	340	68.0	1.167	0.540	83.9	1.167	0.540	187	2491
		214.5	1.104	0.536	261.1	1.104	0.536	185	2455
		43.2	1.196	0.529	56.0	1.196	0.529	187	2494
	286	68.0	1.167	0.540	83.9	1.167	0.540	150	1937
		214.5	1.104	0.536	261.1	1.104	0.536	149	1902
		43.2	1.196	0.529	56.0	1.196	0.529	150	1939
^{238}U	340	73.0	1.131	0.624	80.3	1.131	0.624	187	2416
		17.7	1.267	0.531	15.4	1.267	0.531	187	2408
	286	73.0	1.131	0.624	80.3	1.131	0.624	147	1803
		17.7	1.267	0.531	15.4	1.267	0.531	147	1791
				^{84}Kr projectiles					
^{209}Bi	712	7.68	1.344	0.217	10.0	1.344	0.217	346	2610
		144	1.123	0.560	10.0	1.344	0.217	346	2602
	600	7.68	1.344	0.217	10.0	1.344	0.217	272	1924
		144	1.223	0.560	10.0	1.344	0.217	272	1919

[a] r_R, a_R, r_I, and a_I are the radial parameters used in Eq. (9) to define the real and imaginary potentials, respectively, in Eq. (8).

potential are confirmed. In the present experiments we do not observe such large peak values of $\sigma_{el}/\sigma_{Ruth}$ for the ^{209}Bi+^{84}Kr reaction. Furthermore, the peak values of $\sigma_{el}/\sigma_{Ruth}$ of 1.3 and 1.2 shown in Figs. 5 and 6, respectively, must be considered upper limits due to the possible underestimate of the correction for the transfer events.

In general the radius parameters found from the Fresnel model are larger than the radius parameters of the real optical potential. This difference in radius parameters is not unexpected since in the Fresnel model the radius parameter defines the nuclear separation in a grazing collision, and in the optical model the radius parameter defines a smaller radius corresponding to the overlap of the two nuclei where the nuclear potential has reached 50% of its central value. However, Blair[28] defines a strong absorption radius for the optical model which is analogous to the Fresnel interaction radius and may be written as

$$kR_{SA}=\eta+[\eta^2+l_{1/2}(l_{1/2}+1)]^{1/2}. \quad (12)$$

This strong absorption radius represents the distance of closest approach for the classical Rutherford orbit of angular momentum l, for which the transmission coefficient $T_l=0.5$. The value of R_{SA} is generally constant for all the ambiguous optical potentials which lead to good fits to elastic scattering data. The interaction radius defined by the Fresnel model is also given by an expression similar to Eq. (12) if l_{max} is substituted for $l_{1/2}$, as can be verified by eliminating $\theta_{1/4}$ from Eqs. (4) and (5). The Fresnel interaction radius and R_{SA} thus represent the same classical distance of closest approach, and since for the data discussed in this paper $l_{1/2}=l_{max}$, the strong absorption radius is very close to the interaction radius found from the Fresnel model (Table III).

Brink and Rowley[29] have given some consideration to possible static deformation effects on elastic scattering. Since uranium is known to be deformed, it is possible that deformation effects are present in the elastic scattering data for Ar on U. However, the deformation effects are expected to be small at energies well above the Coulomb barrier and have not been explicitly considered in the analysis described in this paper.

TABLE III. Comparison of parameters found from the optical model and the Fresnel model fit to the data displayed in Figs. 1–6.

	E_{lab}	$R_{int}^{Fresnel}$ (fm)	Optical model R_{SA} (fm)
		Ar projectile	
^{209}Bi	340	13.21	13.30
	286	13.43	13.35
^{238}U	340	13.59	13.60
	286	13.56	13.68
		Kr projectile	
^{209}Bi	712	14.16	14.25
	600	14.24	14.28

Table IV contains parameters deduced from a Fresnel scattering analysis of published heavy ion elastic scattering data.[10–25] Table V compares the values of l_{max} found for the data in Table IV with other optical model analyses of the same data.[17,19] As can be seen from Table V there is good agreement between l_{max} from the Fresnel model and $l_{1/2}$ from the optical model analyses.

B. Optical model parameters

For the ^{40}Ar reactions the optical model potentials tested were restricted to those with four free parameters, V, W, $r_R=r_I$, and $a_R=a_I$. Even then the well known Igo[30] ambiguities are present as evidenced by the potentials listed in Table II. One of the common features of all the potentials derived from fitting elastic scattering of ^{40}Ar on targets of ^{209}Bi or ^{238}U is the similar values of the potential at the strong absorption radius [defined by Eq. (12)]. The average values of the real potential $\langle V_N \rangle$ at R_{SA} for the various potentials listed in Table II for ^{209}Bi and ^{238}U are given in Table VI. The magnitudes of the various imaginary potentials listed in Table II are also the same at the strong absorption radius. With the above restrictions that $r_R=r_I$ and $a_R=a_I$, the magnitudes of the central real and imaginary potentials are comparable. This result is in agreement with the observations of Satchler[24] for ^{12}C, ^{16}O, and ^{20}Ne elastic scattering from ^{208}Pb. For the various potentials tested we found that the fits to the elastic scattering are very insensitive to the values of the real and imaginary potentials for radial distances a few femtometers smaller than R_{SA}.

For the ^{84}Kr reactions the optical model potentials initially examined were again restricted to those with four free parameters. The best fits to the elastic scattering for the ^{209}Bi+^{84}Kr reaction resulted in a class of potentials with similar values of the potential at R_{SA} and with rather small values of the diffuseness parameter. For the potentials we tested, the parameter searches always resulted in diffuseness parameters which were much smaller for ^{84}Kr than those found for ^{40}Ar. The four parameters of one such ^{84}Kr potential are listed in Table II. Equivalent or better fits to the elastic scattering were obtained with a six parameter Woods-Saxon potential including V, r_R, a_R,

TABLE IV. Parameters of the Fresnel model fit to the elastic scattering data of Refs. 10–25.

Reaction	Energy (MeV)	k $(\text{fm})^{-1}$	η	$\theta_{1/4}^{\text{c.m.}}$	r_0 (fm)	$l_{\max}$	σ_R (mb)
$^{12}C + ^{208}Pb$ (Refs. 24 and 25)	96	7.02	27.39	55.5	1.44	52	1791
$^{16}O + ^{54}Fe$ (Ref. 15)	46	4.58	19.3	97.8	1.56	17	478
	48	4.68	18.9	87.6	1.57	20	617
	52	4.87	18.2	75.0	1.57	24	808
$^{16}O + ^{56}Fe$ (Ref. 14)	40	4.30	20.2	143.6	1.56	7	78.7
	50	4.81	18.5	77.7	1.57	23	781
	60	5.27	16.9	56.6	1.57	31	1187
$^{16}O + ^{58}Ni$ (Ref. 16)	44	4.55	21.3	125.6	1.55	11	181
	50	4.85	20.0	90.0	1.55	20	586
	60	5.31	18.2	62.5	1.57	30	1070
$^{16}O + ^{70}Ge$ (Ref. 14)	44	4.72	24.3	145.0	1.59	8	105
	50	5.04	22.8	96.9	1.59	20	557
	60	5.52	20.8	67.9	1.59	31	1053
$^{16}O + ^{74}Ge$ (Ref. 14)	44	4.77	24.3	128.1	1.60	12	227
	48	4.98	23.3	103.5	1.58	18	473
	56	5.38	21.5	70.7	1.63	30	1067
$^{16}O + ^{88}Sr$ (Ref. 16)	52	5.34	26.6	120.0	1.54	15	294
	60	5.73	24.7	83.2	1.52	28	795
$^{16}O + ^{90}Zr$ (Ref. 14)	50	5.25	28.5	167.0	1.56	3	21.2
	60	5.75	26.0	91.0	1.55	26	671
$^{16}O + ^{116}Sn$ (Ref. 13)	66	6.25	31.0	102.0	1.53	25	548
	67	6.29	30.8	96.2	1.55	28	649
$^{16}O + ^{120}Sn$ (Ref. 13)	65.8	6.26	31.1	99.0	1.54	27	606
	66.7	6.29	30.8	95.8	1.54	28	663
$^{16}O + ^{208}Pb$ (Ref. 20)	104	8.29	40.5	82.5	1.46	46	1020
$^{16}O + ^{208}Pb$ (Refs. 24 and 25)	129.5	9.24	36.31	53.1	1.51	73	2015
	192	11.26	29.82	30.8	1.49	108	2944
$^{16}O + ^{235}U$ (Ref. 22)	140	9.69	39.12	56.5	1.45	72.9	1830
$^{20}Ne + ^{197}Au$ (Ref. 21)	208	12.8	38.6	38.5	1.423	110	2376
$^{20}Ne + ^{206}Pb$ (Ref. 21)	208	12.8	40.0	40.0	1.418	110	2344
$^{20}Ne + ^{207}Pb$ (Ref. 21)	208	12.9	40.0	40.0	1.415	110	2340
$^{20}Ne + ^{208}Pb$ (Refs. 24 and 25)	161.2	11.33	45.48	53.1	1.50	91	2071
$^{20}Ne + ^{208}Pb$ (Ref. 21)	208	12.9	40.0	39.5	1.425	111	2400
$^{20}Ne + ^{209}Bi$ (Ref. 21)	208	12.9	40.5	40.0	1.422	111	2374
$^{20}Ne + ^{235}U$ (Ref. 22)	175	11.92	48.99	56.2	1.45	91.8	1900
	252	14.30	40.82	33.8	1.43	134	2810

TABLE IV. (*Continued*)

Reaction	Energy (MeV)	k (fm)$^{-1}$	η	$\theta_{1/4}^{c.m.}$	r_0 (fm)	l_{max}	σ_R (mb)
^{32}S + ^{24}Mg	75	4.59	19.7	110.0	1.58	14	327
(Ref. 17)	90	5.03	18.0	80.0	1.52	21	623
	110	5.56	16.3	54.8	1.55	32	1093
	120	5.81	15.6	46.0	1.58	37	1323
^{32}S + ^{27}Al	73	4.84	21.7	115.0	1.60	14	294
(Ref. 17)	85	5.22	20.1	84.2	1.55	22	620
	110	5.94	17.1	55.0	1.52	34	1084
^{32}S + ^{40}Ca	82.5	6.24	31.4	135.0	1.59	13	158
(Ref. 17)	85	6.34	30.9	120.0	1.59	18	276
	90	6.52	30.0	102.0	1.59	24	473
^{40}Ar + ^{109}Ag	169	13.1	64.8	88.0	1.46	67	850
(Ref. 23)	197	14.2	60.0	65.0	1.47	94	1410
	236	15.6	54.9	50.0	1.45	118	1830
	288	17.2	49.7	39.0	1.40	140	2110
	337	18.6	45.4	32.5	1.38	157	2270
^{40}Ar + ^{121}Sb	282	17.4	54.4	41	1.44	145	2210
(Ref. 23)	340	19.1	49.6	32	1.43	173	2600
^{40}Ar + ^{209}Bi	286	19.6	87.9	60.0	1.43	151	1887
	340	21.4	80.6	47.0	1.41	185	2382
^{40}Ar + ^{238}U	286	20.0	97.4	68.0	1.41	144	1648
	340	21.8	87.4	51.0	1.41	187	2336
^{84}Kr + ^{65}Cu	494	19.4	67.8	48	1.44	152	1950
(Ref. 23)	604	21.5	61.2	36	1.44	188	2430
^{84}Kr + ^{181}Ta	457	29.3	177	113.0	1.33	118	515
(Ref. 18)							
^{84}Kr + ^{197}Au	457	30.0	192	131.0	1.31	88	273
(Ref. 18)							
^{84}Kr + ^{208}Pb	500	31.9	190	97.7	1.35	166	866
(Refs. 10 and 11)	500	31.9	190	101.0	1.33	157	769
^{84}Kr + ^{209}Bi	600	35.2	176	66.0	1.38	270	1880
	712	38.2	162	50.5	1.37	343	2533
^{84}Kr + ^{232}Th	500	32.9	210	125.0	1.28	109	351
(Ref. 11)							
^{84}Kr + ^{238}U	456	31.6	223	168.0	1.34	24	19
(Ref. 12)							

W, r_I, and a_I. The real potential for this class of potentials was not limited to those with small values of a_R but only had the restriction of similar values of the real potential at R_{SA}. One such six parameter potential is listed also in Table II. All of the potentials found to give the better fits to the ^{84}Kr elastic scattering required the imaginary potential to have small values of a_I ($\sim\frac{1}{4}$ fm) and corresponding rather large values of r_I. However, real potentials with a variety of values of V, r_r, and a_r give essentially equivalent fits to the elastic scattering data as long as the real potentials at R_{SA} are approximately the same.

In summary it should be emphasized that the Woods-Saxon potentials listed in Table II are representative of those found during our limited number of calculations and are in no way to be considered an exhaustive list.

C. Variations of r_0 with Z_1Z_2

The variation of the radius parameter r_0 with the product Z_1Z_2 is shown in Fig. 8 for the reactions listed in Table IV. Similar correlations have been made previously[31,32] of the radius parameter r_0 as

TABLE V. Comparison of the Fresnel prediction for l_{max} with the optical model value of $l_{1/2}$.

Reaction	Lab energy (MeV)	Fresnel l_{max}	$l_{1/2}$
$^{32}S+^{24}Mg$	75	14	13 [a]
	90	21	22 [a]
	110	32	31 [a]
	120	37	36 [a]
$^{32}S+^{27}Al$	73	14	16 [a]
	85	22	22 [a]
	110	34	33 [a]
$^{32}S+^{40}Ca$	82.5	13	14 [a]
	85	18	18 [a]
	90	24	23 [a]
$^{40}Ar+^{77}Se$	146	52	56 [b]
$^{40}Ar+^{209}Bi$	286	151	150 [c]
	340	185	186 [c]
$^{40}Ar+^{238}U$	286	144	147 [c]
	340	187	187 [c]
$^{84}Kr+^{209}Bi$	600	270	272 [c]
	712	343	346 [c]

[a] Data of Gutbrod *et al.*, Ref. 17 (optical model).
[b] Data of Galin *et al.*, Ref. 19 (optical model).
[c] This paper (optical model).

a function of η and Z_1Z_2. Since the correlation of r_0 with η contains an implicit energy dependence for r_0, we have chosen to show the correlation of r_0 with Z_1Z_2 as existing data do not clearly show that r_0 is dependent on the projectile energy. The data of Fig. 8 may be used to estimate the total reaction cross section for an unmeasured heavy ion reaction. The procedure for prediction of the total reaction cross section is to first estimate r_0 from the data of Fig. 8 for the Z_1Z_2 value appropriate to the projectile and target combination. Then, this value of r_0 is used to calculate an estimated quarter-point angle $\theta_{1/4}$ from Eq. (5). The resulting value of $\theta_{1/4}$ is substituted into Eq. (4) to obtain an estimate of l_{max}, and finally the estimated l_{max} is used in Eq. (6) to calculate the total reaction cross section. The accuracy of a total reaction cross section estimated by this method is better than ±20% for projectiles and energies for which the Fresnel model is valid.

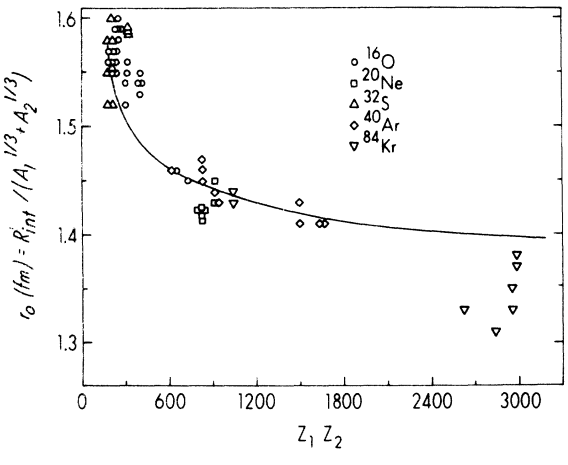

FIG. 8. Plot of the interaction radius parameter r_0 [where $r_0 = R_{int}/(A_1^{1/3}+A_2^{1/3})$] as a function of z_1z_2 for various projectile-target combinations. The solid line is calculated with Eq. (13).

The line drawn in Fig. 8 is calculated with the formula

$$r_0 = [C_1 + C_2 + S(\tfrac{1}{4})]/(A_1^{1/3} + A_2^{1/3}), \qquad (13)$$

where $C_1 + C_2$ are the electron scattering half-density radii[33] from a two-parameter Fermi distribution function, and $S(\frac{1}{4})$ is a constant of 3.2 fm. The fact that several configurations of target and projectile with similar values of Z_1Z_2 are possible means that individual calculated values of r_0 are spread about the line drawn in Fig. 8. One observes from this figure that the variation in r_0 based on the experimentally measured values of the interaction radius R_{int} [where $r_0 = R_{int}/(A_1^{1/3} + A_2^{1/3})$] is qualitatively reproduced by Eq. (13). This suggests that heavy ion nuclear reactions are initiated at a fixed distance between the half-density radii of the two nuclei as illustrated in Fig. 9. The uncertainty in the distance $S(\frac{1}{4})$ is ~0.3 fm. An uncertainty of this magnitude transforms into a change of 0.05 fm in the calculated value of r_0 at small Z_1Z_2 and a change of 0.03 fm at large values of Z_1Z_2. With an error in $S(\frac{1}{4})$ of 0.03 fm some of the experimental points in the neighborhood of $Z_1Z_2 = 3000$ are still slightly smaller than the calculated values of r_0. This may indicate that the distance $S(\frac{1}{4})$ for the krypton induced reactions on heavy targets is slightly smaller than 2.9 fm. Alternatively, most of the experimental values of r_0 determined from elastic scattering measurements may be too small due to the fact that the correction for non-elastic processes in most of the existing krypton measurements is underestimated.

If the diffuseness parameter in the Fermi density distribution is assumed to be in the range 0.5 to 0.6 fm,[33] the value of ρ/ρ_0 at $S(\frac{1}{4}) = 3.2 \pm 0.3$ fm is 0.05 ± 0.02. The result that nuclear reactions are initiated when each ion overlaps the other to about 5% of its central density is approximate insofar as the density distribution of each of the heavy ions may not follow a Fermi distribution out to the radii considered here.

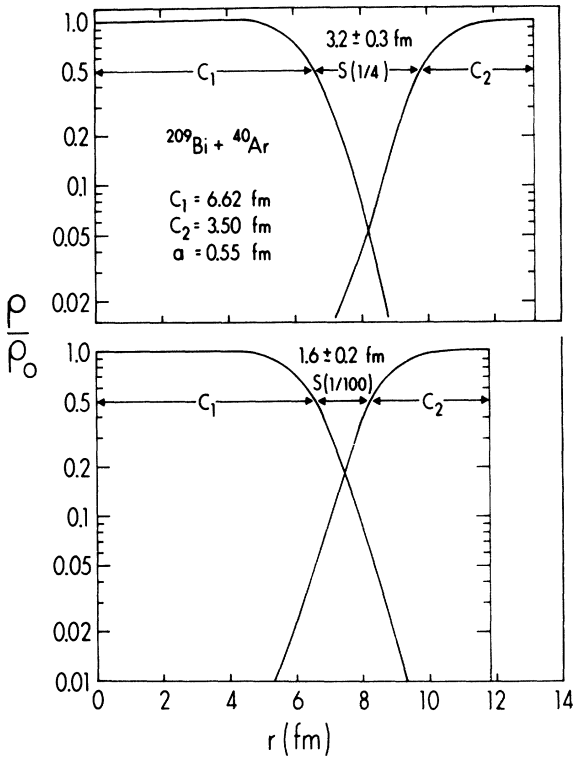

FIG. 9. Plot of the ratio of the nuclear density to the central nuclear density of each heavy ion as a function of the interaction distance between the two ions. It is assumed that the density distribution of each ion is given by a two parameter Fermi distribution function. For the one-quarter point, where $\sigma_{el}/\sigma_{Ruth}=1/4$, the quantity $S(1/4)$ is a constant of 3.2 ± 0.3 fm and independent of reacting ions. The corresponding value of ρ/ρ_0 is 0.05 ±0.02. The bottom part of the figure corresponds to the one-hundredths point, where $\sigma_{el}/\sigma_{Ruth}=1/100$. The value of $S(1/100)$ is 1.6 ± 0.2 fm and corresponds to a value of $\rho/\rho_0\simeq0.20\pm0.05$.

D. Estimate of Woods-Saxon potential parameters V_0 and a from elastic and the liquid drop model

It is well known that heavy ion elastic scattering measurements determine the real potential at large radial distances near the interaction radius. Although it is possible to obtain information on the radial dependence of V by varying the projectile energy,[34] the radial range available to investigation is very small for heavy ions. An alternate approach to this problem is to utilize the elastic scattering data in conjuction with the liquid drop model.

In the liquid drop model the maximum nuclear force is obtained at the touching distance, which for two spherical nuclei is given by[35]

$$\left(\frac{dV_N}{dr}\right)_{r=R}=\frac{2\pi(\gamma_1+\gamma_2)R_1R_2}{R}, \tag{14}$$

where $\gamma=0.9517[1-1.7826(N-Z/A)^2]$, $R=R_1+R_2$, and R_1 and R_2 are the radii of the target and projectile nuclei, respectively,

$$R_i=(1.13+0.0002A_i)A_i^{1/3}\times[1-(1.13+0.0002A_i)^{-2}A_i^{-2/3}]. \tag{15}$$

If the above value of the nuclear force is equated to the force found for a Woods-Saxon potential at $r=R$ then one obtains a relation[31] between V_0 and the diffuseness parameter a

$$\left(\frac{dV_N}{dr}\right)_{r=R}=-\frac{V_0}{4a}. \tag{16}$$

Use of Eq. (16) along with the value of $\langle V_N\rangle$ determined at the strong absorption radius R_{SA} from the optical model fits to the elastic scattering allows one to deduce the parameters V_0 and a [assuming a Woods-Saxon type potential for which R is given by Eq. (15) as listed in Table VI]. For the reactions of this paper the values of V_0 and a estimated by this procedure are shown in Table VI. The potentials derived in this way give optical model fits to the data which are of a similar quality to the potentials listed in Table II. The potential derived in this way may be a reasonable estimate over the radial distance from R_{SA} to the radius where the nuclear force dV_N/dr, has its maximum value. As the radial distance is further decreased the potential may become repulsive as the two nuclei penetrate each other. Such a repulsion is a natural consequence of keeping the interaction degrees of freedom frozen as, for example, in the proximity potential or the energy density potential.[36-39]

An interaction potential for heavy ion scattering

TABLE VI. Values of V_0 and a determined by combining the elastic scattering data and the liquid drop model.

Reaction	R_{SA} (fm)	R at $\left(\frac{dV_N}{dr}\right)_{max}$	$\langle V_N\rangle$ at R_{SA} (MeV)	V_0 (MeV)	a (fm)
^{209}Bi + ^{40}Ar	13.33	10.445	−0.77	−69	0.64
^{238}U + ^{40}Ar	13.64	10.796	−0.97	−72	0.66
^{209}Bi + ^{84}Kr	14.27	11.634	−1.10	−79	0.62

has often been estimated by folding the density distribution of the projectile with the real part of the single-nucleon optical potential of the target nucleus. Using this type of folded potential, Brink and Rowley[29] deduced a radial parameter of the folded potential by matching the calculated value of l_{max} with the value of l_{max} determined from a Fresnel analysis of the experimental elastic scattering cross sections using the one-quarter-point method [Eqs. (1) – (4)]. The difficulty with the Brink-Rowley procedure is the assumption that l_{max} can be calculated from the position of the maximum in the total potential energy $V(l,r)$ at some radial distance by equating this maximum potential energy to the center-of-mass energy. For very heavy projectiles the total potential energy $V(l,r)$ probably does *not* have a radial maximum for large angular momenta near l_{max}. Therefore, use of the Brink-Rowley procedure produces a nuclear potential strong enough to force a maximum in $V(l_{max},r)$ at some radius, and hence, such a procedure gives an unrealistically deep nuclear potential for very heavy ion interactions.[31]

E. Semi classical model analysis

The gross features of heavy ion elastic scattering are described qualitatively by a semiclassical model.[40] Such a description is applicable since $\eta = D(\theta=\pi)/2\lambda$ has values for the present experiments of approximately 85 (for ^{40}Ar) and 170 (for ^{84}Kr). Here $D(\theta=\pi)$ is the distance of closest approach in a head-on collision (neglecting the nuclear field) and λ is the reduced wavelength at infinite ion separation.

In Fig. 10 are plotted the elastic to Rutherford scattering cross section ratios, $\sigma_{el}/\sigma_{Ruth}$ for the ^{209}Bi + ^{40}Ar reaction as a function of the distance $d(\theta)$, where $d(\theta) = D(\theta)/(A_1^{1/3} + A_2^{1/3})$ and $D(\theta)$ is the distance of closest approach for a Rutherford trajectory with scattering angle θ. The distance $D(\theta)$ is given by

$$D(\theta) = \frac{Z_1 Z_2 e^2}{2E}\left(1 + \csc\tfrac{1}{2}\theta\right)$$

$$= \eta\lambda\left(1 + \csc\tfrac{1}{2}\theta\right). \qquad (17)$$

As $d(\theta)$ or $D(\theta)$ decreases, corresponding to an increase in angle θ, the projectile comes into a region where it experiences the attractive nuclear potential and is deflected to smaller angles. The use of the parameter $d(\theta)$ allows one to describe the elastic scattering of ^{40}Ar on ^{209}Bi at our two energies by the expression

$$\frac{\sigma_{el}}{\sigma_{Ruth}} = 1 - P_{reac}(d), \qquad (18)$$

where

$$P_{reac}(d) = \begin{cases} 0 & \text{for } d(\theta) \geq d_0 \\ 1 - \exp\left(\dfrac{[d(\theta) - d_0](A_1^{1/3} + A_2^{1/3})}{\Delta}\right) & \text{for } d(\theta) < d_0 \end{cases} \qquad (19)$$

with $d_0 = 1.495$ fm and $\Delta = 0.47$ fm. These values are to be compared to $d_0 = 1.68$ fm and $\Delta = 0.55$ fm obtained for ^{12}C and ^{16,18}O scattering on a number of targets ($A = 40$ to 96).[40]

In Fig. 11 a similar plot is made for the ^{238}U + ^{40}Ar reaction. Values of d_0 and Δ are 1.47 fm and 0.46 fm, respectively, for the ^{238}U + ^{40}Ar reaction in rather close agreement with similar values found for the ^{209}Bi + ^{40}Ar reaction. However, the ^{238}U + ^{40}Ar reaction appears to have more of a knee with the actual values of $\sigma_{el}/\sigma_{Ruth}$ dropping below one at values of d less than 1.54. The values of d_0 and Δ are somewhat smaller for the ^{209}Bi + ^{84}Kr reaction, although the uncertainties in these quantities are large for this reaction. For the ^{40}Ar reactions the error introduced in d_0 by the uncertainty in the contributions of transfer events in the energy spectra is less than 0.03 fm. The reduction of d_0 with increasing values of $Z_1 Z_2$ is analogous to the reduction of

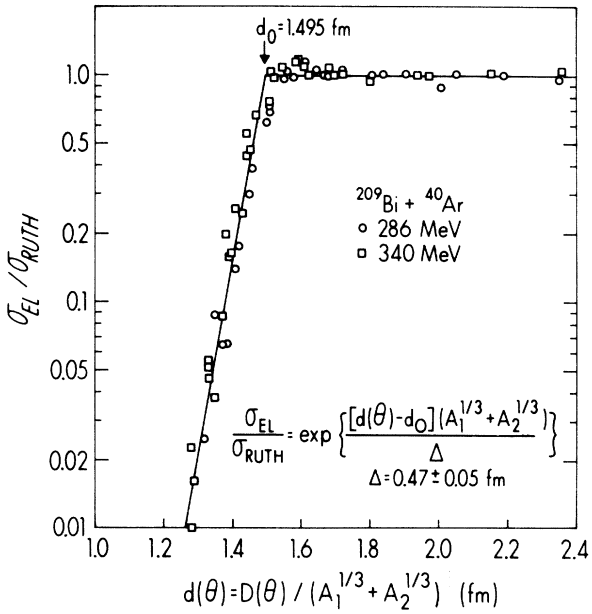

FIG. 10. Ratios of the elastic to Rutherford cross sections for the ^{209}Bi + ^{40}Ar reaction at 340 and 286 MeV as a function of the distance $d(\theta)$ [where $d(\theta) = D(\theta)/(A_1^{1/3} + A_2^{1/3})$]. The quantity $D(\theta)$ is defined in Eq. (17) and is the distance of closest approach for a Rutherford trajectory with scattering angle θ.

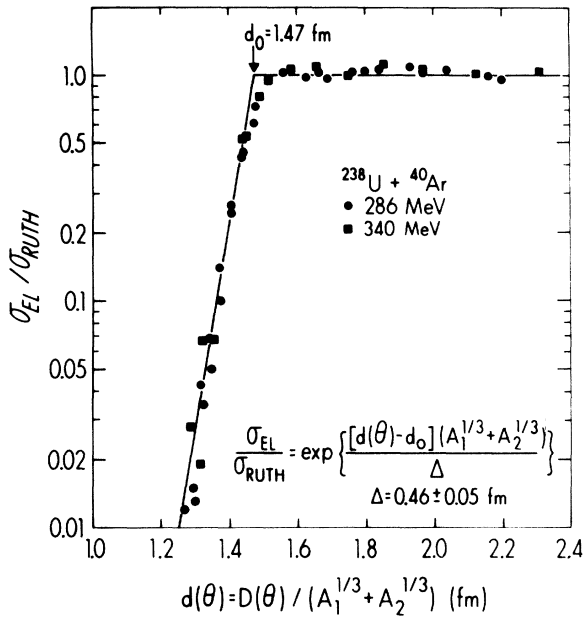

FIG. 11. Same as Fig. 10 except for the ^{238}U + ^{40}Ar reaction.

r_0 [when the interaction radius is parametrized in terms of $r_0(A_1^{1/3}+A_2^{1/3})$] with Z_1Z_2 as discussed earlier.

Values of $D(1/100)$ have been calculated from the present data displayed in Figs. 10 and 11 and from data[40] reported in the literature. The quantity $D(1/100)$ is evaluated from Eq. (18) and is defined as the distance of closest approach between the two nuclei at the angle θ where the ratio $\sigma_{el}/\sigma_{Ruth}$ is equal to 0.01. If one interprets these data in analogy to the one-quarter-point distances discussed earlier (see Fig. 8) such that

$$D(1/100) = C_1 + C_2 + S(1/100), \tag{20}$$

one finds that $S(1/100)$ is approximately equal to 1.6 ± 0.2 fm and independent of Z_1Z_2 [as was $S(\frac{1}{4})$]. Again assuming a diffuseness parameter in the range of 0.50 to 0.60 fm, the corresponding value of ρ/ρ_0 for $S(1/100) = 1.6$ fm is 0.20 ± 0.05. At these smaller distances of $D(1/100)$ the projectile experiences the attractive nuclear potential more strongly and larger deviations are expected from the classical Rutherford trajectories. Even so, for all heavy ion reactions examined the value of $\sigma_{el}/\sigma_{Ruth} = 0.01$ or $P_{reac}(d) = 0.99$ is reached at approximately the same value of ρ/ρ_0.

CONCLUSION

Analysis of elastic scattering data is complicated by the presence of few nucleon transfer events which give rise to scattered particles of energy close to the energy of the elastically scattered projectile. Hence, it is essential that data be collected with a high energy resolution if the detailed shape of the elastic scattering angular distribution is to be examined. Because of the rapid decrease in the ratio $\sigma_{el}/\sigma_{Ruth}$ near the quarter point, it is still possible to extract from elastic scattering values of the total reaction cross section for heavy ion reactions to within ±10%, even from data taken with moderate energy resolution (~2%).

The comparison of optical and Fresnel scattering models used to fit heavy ion elastic scattering data indicates that the Fresnel model reproduces the gross features of the elastic scattering angular distributions at angles not too far from the quarter point. For heavy ions the Fresnel model leads to reasonable estimates of the maximum angular momentum for reacting ions and the total reaction cross section. Further, the Fresnel interaction radii are in good agreement with the optical model strong absorption radii.

The systematics of the variation of the Fresnel interaction radii indicate that the probability of nuclear reactions between heavy ions is a universal function of the separation of their surfaces. Assuming a two-parameter Fermi density distribution for each of the heavy ions with a half-density radius of C_i, the onset of nuclear reaction between heavy ions occurs at a constant separation distance of 3.2 ± 0.3 fm, where the Fresnel interaction radius is given by $R_{int} = C_1 + C_2 + 3.2$ fm. With a diffuseness parameter of 0.55 fm in the Fermi density distribution, the onset of nuclear reaction between heavy ions is also describable in terms of a universal function of the ratio of the maximum overlap density to the central nuclear density of approximately 5% for each ion.

The radial dependence of the real nuclear potential is obtained from a combination of the nuclear potential at the strong absorption radius derived from optical model fitting of the elastic scattering and the maximum nuclear force between heavy ions as predicted by the liquid drop model. Such a potential may be a reasonable estimate of the internuclear potential at nuclear separation between the liquid drop touching distance and the strong absorption radius.

ACKNOWLEDGMENTS

The authors thank A. Ghiorso, H. Grunder, R. Eppley, and the operating crew of the superhilac accelerator for their assistance in these experiments. We also thank R. DeVries for his assistance with the optical model code.

*Permanent address: Western Australian Institute of Technology, Perth, Western Australia.

†Work supported in part by the U.S. Energy Research and Development Administration.

[1]A. G. Artukh, G. F. Gridnev, V. L. Mikheev, V. V. Volkov, and J. Wilczyński, Nucl. Phys. A215, 91 (1973).

[2]F. Hanappe, M. Lefort, C. Ngô, J. Péter, and B. Tamain, Phys. Rev. Lett. 32, 738 (1974).

[3]K. L. Wolf, J. P. Unik, J. R. Huizenga, J. R. Birkelund, H. Freiesleben, and V. E. Viola, Phys. Rev. Lett. 33, 1105 (1974).

[4]S. G. Thompson, L. G. Moretto, R. C. Jared, R. P. Babinet, J. Galin, M. M. Fowler, R. C. Gatti, and J. B. Hunter, Physica Scripta 10A, 36 (1974).

[5]F. Hanappe, C. Ngô, J. Péter, and B. Tamain, in *Proceedings of the International Conference on Reactions between Complex Nuclei, Nashville, Tennessee, 10 – 14 June 1974,* edited by R. L. Robinson, F. K. McGowan, J. B. Ball, and J. H. Hamilton (North-Holland, Amsterdam/American Elsevier, New York, 1974).

[6]J. Péter, C. Ngô, and B. Tamain, J. Phys. Paris Lett. 36, 23 (1975).

[7]W. E. Frahn and R. H. Venter, Ann. Phys. (N.Y.) 24, 243 (1963).

[8]W. E. Frahn, Phys. Rev. Lett. 26, 568 (1971); Ann. Phys. (N.Y.) 72, 524 (1972).

[9]J. S. Blair, Phys. Rev. 95, 1218 (1954).

[10]R. Vandenbosch, M. P. Webb, and T. D. Thomas, in *Proceedings of the Symposium on Classical and Quantum Mechanical Aspects of Heavy Ion Reactions, Heidelberg, Germany, 1974* (Springer-Verlag, Berlin, 1975).

[11]P. Colombani, J. C. Jacmont, N. Poffe, M. Riori, C. Stéphan, and J. Tys, Phys. Lett. 42B, 197 (1972).

[12]M. Lefort, C. Ngô, J. Péter, and B. Tamain, Nucl. Phys. A197, 485 (1972).

[13]B. C. Robertson, J. T. Sample, D. R. Goosman, K. Nagatani, and K. W. Jones, Phys. Rev. C 4, 2176 (1971).

[14]A. W. Obst, D. L. McShan, and R. H. Davis, Phys. Rev. C 6, 1814 (1972).

[15]P. Bonche, B. Giraud, A. Cunsolo, M. C. Lemaire, M. C. Mermaz, and J. L. Quebert, Phys. Rev. C 6, 577 (1972).

[16]P. R. Christensen, I. Chernov, E. E. Gross, R. Stokstad, and F. Videbaek, Nucl. Phys. A207, 433 (1973).

[17]H. H. Gutbrod, M. Blann, and W. G. Winn, Nucl. Phys. A213 285 (1973).

[18]P. Colombani, Ph.D. thesis, Orsay, France, 1974 (unpublished).

[19]J. Galin, B. Gatty, D. Guerreau, C. Rousset, K. C. Schlotthauer-Voos, and X. Tarrago, Phys. Rev. C 9, 1113 (1972).

[20]F. D. Becchetti, D. G. Kovar, B. G. Harvey, J. Mahoney, B. Mayer, and F. G. Pühlofer, Phys. Rev. C 6, 2215 (1972).

[21]H. L. Reynolds, E. Goldberg, and D. D. Kerlee, Phys. Rev. 119, 2009 (1960).

[22]V. Viola (private communication).

[23]M. Blann (private communication).

[24]G. R. Satchler, Phys. Lett. 55B, 167 (1975).

[25]J. B. Ball, G. B. Fulmer, E. E. Gross, M. L. Halbert, D. C. Hensley, C. A. Ludeman, M. J. Saltmarsh, and G. R. Satchler, Nucl. Phys. A252, 208 (1975).

[26]F. G. Perey (unpublished).

[27]N. Rowley, Nucl. Phys. A239, 134 (1975).

[28]J. S. Blair, in *Lectures in Theoretical Physics* (Univ. of Colorado Press, Boulder, 1966), Vol. VIII C; B. Fernandez and J. S. Blair, Phys. Rev. C 1, 523 (1970).

[29]D. M. Brink and N. Rowley, Nucl. Phys. A219, 79 (1974); N. Rowley, *ibid.* A219, 93 (1974).

[30]G. Igo, Phys. Rev. 115, 1665 (1959).

[31]J. R. Huizenga, University of Rochester Report No. UR-NSRL-90 (unpublished); Nukleonika 20, 291 (1975).

[32]L. C. Vaz and J. M. Alexander, Phys. Rev. C 10, 464 (1974); J. M. Alexander, H. Delagrange, and A. Fleury, *ibid.* 12, 149 (1975).

[33]C. W. Jager, H. deVries, and C. deVries, At. Data Nucl. Data Tables 14, 479 (1974).

[34]D. A. Goldberg and S. M. Smith, Phys. Rev. Lett. 33, 715 (1974).

[35]J. Wilczyński, Nucl. Phys. A216, 386 (1973).

[36]J. Randrup, W. J. Swiatecki, and C. F. Tsang, Berkeley Report No. LBL-3603, December 1974 (unpublished).

[37]J. Galin, D. Guerreau, M. Lefort, and X. Tarrago, Phys. Rev. C 9, 1018 (1974); C. Ngô, B. Tamain, J. Galin, M. Beiner, and R. J. Lombard, Nucl. Phys. A240, 353 (1975); C. Ngô, B. Tamain, R. J. Lombard, D. Mas, and H. H. Deubler, Nucl. Phys. A252, 237 (1975).

[38]K. A. Breuckner, J. Buchler, and M. M. Kelly, Phys. Rev. 173, 944 (1968).

[39]R. J. Lombard, Ann. Phys. (N.Y.) 77, 380 (1973).

[40]P. R. Christensen, V. I. Manko, F. D. Becchetti, and R. J. Nickles, Nucl. Phys. A207, 33 (1973).